21st Australasian Fluid Mechanics Conference
Adelaide, Australia
10-13 December 2018

Wake of a DST Submarine Model captured by Stereoscopic Particle Image Velocimetry

S.-K. Lee, P. Manovski and C. Kumar

Defence Science and Technology Group, Melbourne, VIC 3207 AUSTRALIA

Abstract

This paper describes low-speed wind-tunnel testing of a new 2 m long Defence Science and Technology generic conventional submarine model by stereoscopic particle image velocimetry (SPIV). The aim is to capture three components of velocity for a model side-slip of 10° at model-length Reynolds numbers of 4×10^6 and 8×10^6 to allow study of the submarine wake.

From ensemble averages of 3000 SPIV image pairs, the most striking flow feature is on the upper hull of the new model. It is a system of three co-rotating vortices produced by a cruciform appendage which consists of a vertical fin and two horizontal hydroplanes. Cross-sectional SPIV at 51.1%, 65.0% and 81.5% of the model length (L) indicates that vortex circulation is strongest from the fin, followed by the windward hydroplane then the leeward hydroplane. Increasing the Reynolds number from 4×10^6 to 8×10^6 increases circulation of the vortex system by $\simeq 3\%$ and shifts the fin wake leeward by up to $0.5\%L$.

Introduction

The Defence Science and Technology (DST) generic conventional submarine model tested here is based on a conceptual design by Joubert [5]. It was established by the DST Group Maritime Division to foster international cooperation on bench-marking and validation studies of submarine hydrodynamics. Work began in the early 2010s, which involved testing of a 1.35 m long Joubert model in the DST low-speed wind tunnel. The testing included 2-component particle image velocimetry [6], surface-pressure measurements [4] and flow visualisation [7] to provide experimental data to guide numerical modelling [1, 2]. It primarily captured the wake at a model side-slip or yaw angle of 10° to assist interpretation of large-scale flow separation in a submarine manoeuvre.

A recent design study [9] offered some insights into the manoeuvring behaviour of the Joubert model, and this led to a few geometric modifications to improve the directional stability of the model. The modified geometry is known as 'BB2', after [9]. Given that key changes involved a new vertical fin and two horizontal fin hydroplanes on the upper hull, there is a need to characterise the wake produced by this cruciform appendage to assist on-going studies.

This is the first SPIV investigation of the wake flow produced by the new DST submarine model (BB2), where the model is tested at a yaw angle (ψ) of 10° and at high Reynolds numbers.

DST Generic Model (BB2) for Wind-Tunnel Testing

Figure 1 shows the new geometry of the DST submarine model. The model used for this test has a fixed length (L) of 2 m and a length-to-diameter ratio of 7.3. It is axisymmetric for the first $7.0\%L$, where the nose shape is derived from a NACA-0018 forebody. On the casing, the fin shape is that of NACA-0022 with a height of $8.0\%L$ and a chord length of $15.7\%L$. On the fin, there are two NACA-0015 horizontal hydroplanes with a combined span of $11.7\%L$ and a root chord of $3.3\%L$. The leading edge of each hydroplane is swept at 9.3°, where the ratio between the root chord and the tip chord is 0.77.

The longitudinal distance is $28.3\%L$ from the tip of the nose to the leading edge of the fin, and is $29.6\%L$ from the tip of the nose to the leading edge of the hydroplanes. The hydroplanes are located at $5.6\%L$ above the casing. For further details of the geometry, see [5, 9].

The model (see figure 1) is truncated at $95\%L$ for sting-mounted testing in the DST low-speed wind tunnel. The tunnel is a closed-loop facility driven by a 660 kW, 3.96 m diameter, 8 blade fan, and the test section is 2.743 m wide, 2.134 m high and 6.553 m long. For this test, the freestream velocities (U_∞) are $\simeq 29$ m/s and $\simeq 61$ m/s, which correspond to body-length Reynolds numbers ($Re_L = LU_\infty/\nu$, where ν is the kinematic viscosity of air) of 4×10^6 and 8×10^6.

To trip the flow over the hull, a circumferential ring of trip dots (diameter of 1.27 mm and center-to-center spacing of 2.54 mm) is located on the model at $5\%L$. The height of the trip dots is 0.29 mm and 0.15 mm for the Reynolds numbers of 4×10^6 and 8×10^6, respectively. The fin and the hydroplanes are untripped. The method of sizing the trip dots is from [3].

SPIV Measurement Technique

To perform SPIV, the flow is seeded with $\simeq 1$ μm diameter (di-ethyl-hexyl-sebacat) oil droplets at concentration of 20 to 30 mg/m^3 and the seeding is illuminated by a dual-cavity Litron Nd:YAG laser (8 ns pulse at $\simeq 425$ mJ). To minimise stray reflections, the model and the test-section walls are painted black. By orientating the laser-sheet normal to the streamwise x direction, this allows the cross-sectional flow to be captured by a pair of LaVision digital cameras (6600 by 4400 pixels with CCD resolution of 5.5 μm/pixel). The cameras are located outside the test section and are fitted with a 200 mm lens set at f-stop$=5.6$ to provide an adequate depth-of-field. The reproduction ratio is $\simeq 10$ and the useful field-of-view is up to 280 mm by 180 mm (or $0.14L$ wide by $0.09L$ high). The cameras are arranged symmetrically about the laser-sheet at oblique angles of $\simeq 45^\circ$ (figure 1) and a tilt-and-shift technique is used to allow sharp corner-to-corner focusing and to reduce vignetting [8].

To ease alignment and targeting, the cameras, laser and laser-sheet forming optics are mounted on a common optical bench. By traversing the bench in the vertical z direction, the field-of-view captures the flow over the upper hull, mid hull and the lower hull at a fixed streamwise location of the model. To capture the flow at different streamwise x locations, the model is translated forward or backward on a floor rail in the test section. The measurement locations are at $51.1\%L$, $65.0\%L$ and $81.5\%L$; see figures 1 and 2.

SPIV Data Processing

To correlate successive SPIV images, the laser-sheet is set at a fixed thickness $\Delta x_{\text{laser}} \simeq 3.5$ mm, and the laser-pulse delay time (Δt_{pulse}; typically in a few microseconds) is adjusted via a programmable timing unit (LaVision PTU X) such that $\Delta t_{\text{pulse}} \lesssim 0.3\Delta x_{\text{laser}}/U_\infty$. The images are calibrated with a two-sided (LaVision 309-15) target and the velocity field is computed by using the commercial DaVis 8.3 software.

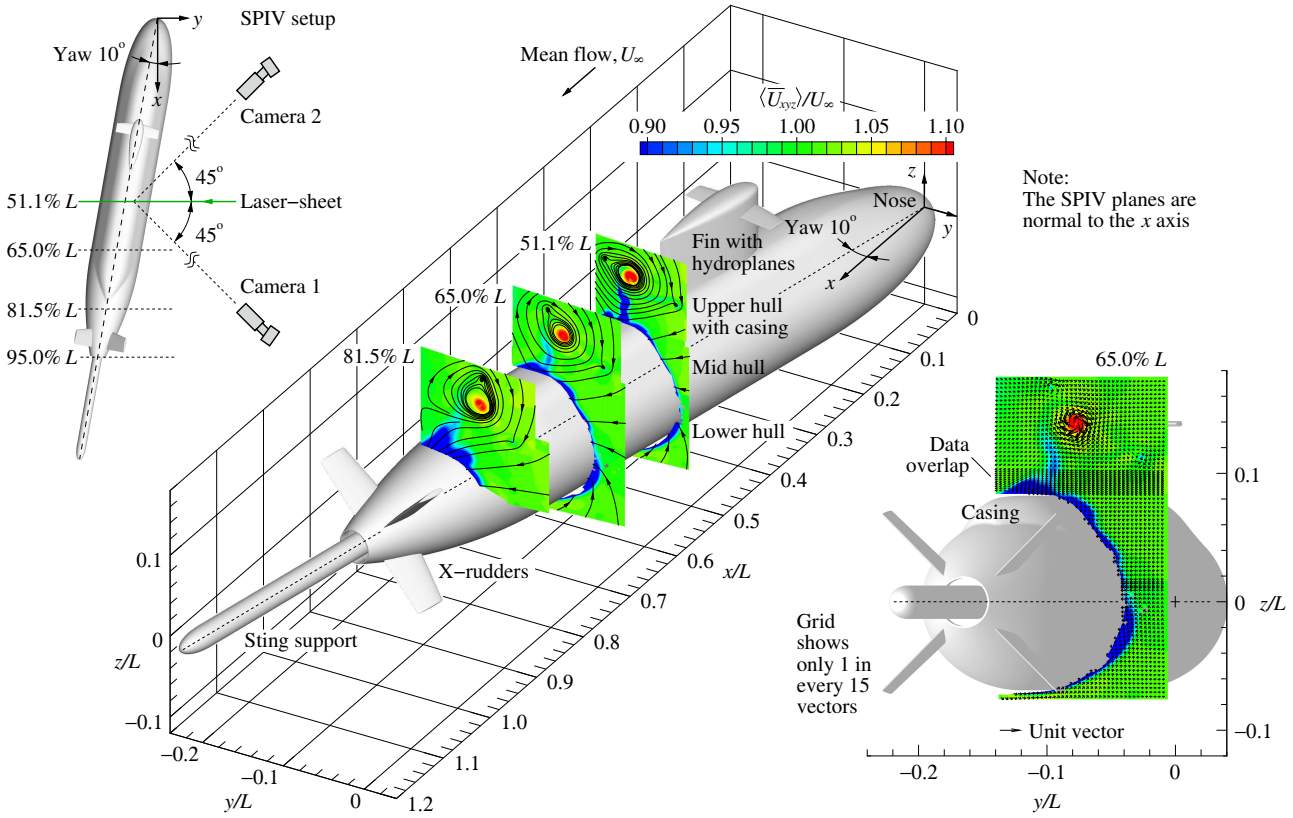

Figure 1. The DST generic conventional submarine model at 10° yaw starboard and the leeward SPIV measurement planes; $Re_L = 4 \times 10^6$.

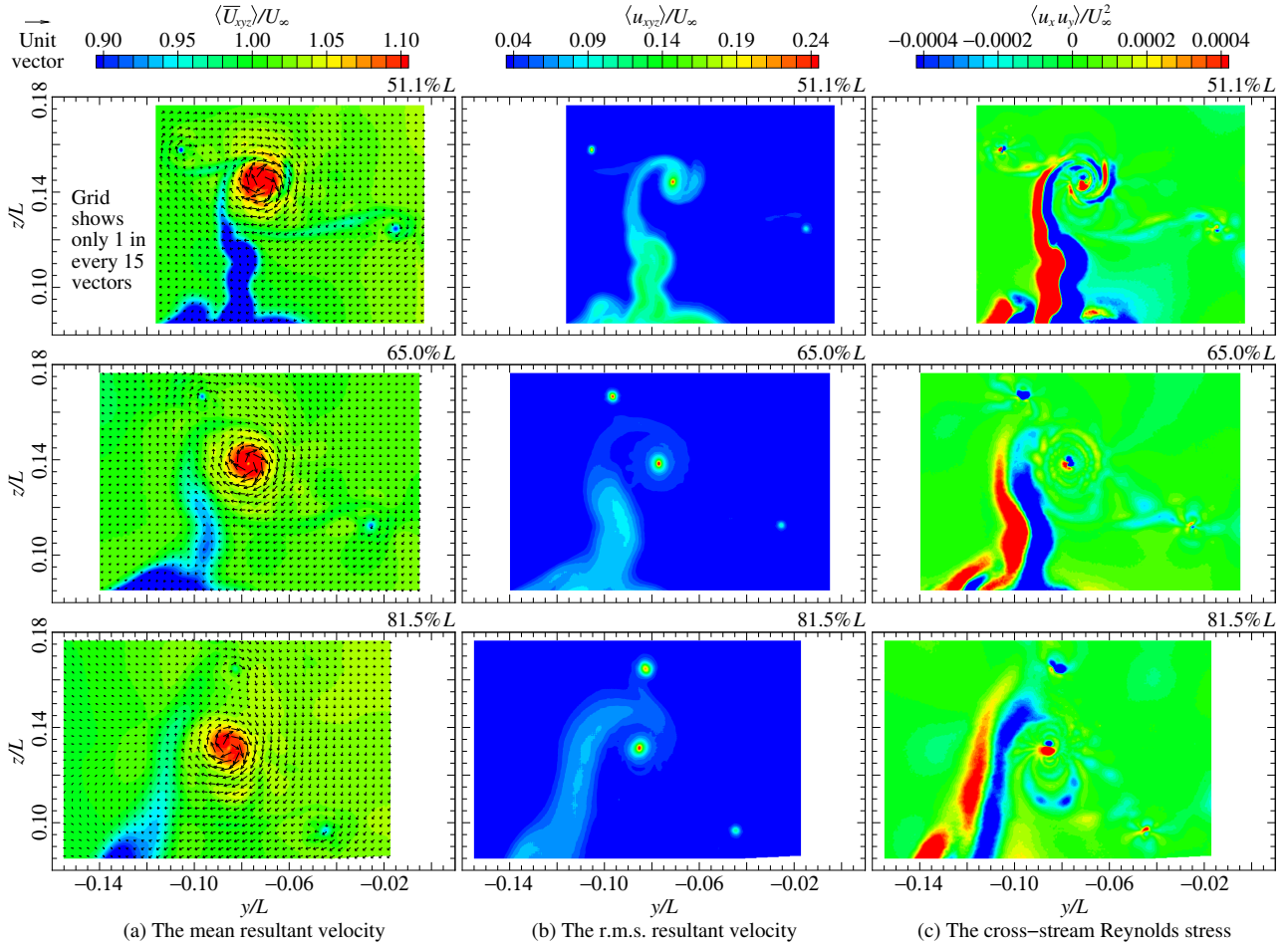

(a) The mean resultant velocity (b) The r.m.s. resultant velocity (c) The cross−stream Reynolds stress

Figure 2. Ensemble-averaged flow field on the upper hull of the submarine at 10° yaw; $Re_L = 4 \times 10^6$.

DaVis determines the distribution of cross-correlation values and stores the four highest correlation peaks found in each interrogation window, where these peaks are determined after the elimination of background noise. To ensure that the same seeding particles are correlated and that there is adequate spatial resolution of the velocity field, the correlation values are iterated twice with decreasing size of the interrogation windows. Initial size is 64×64 pixels at 50% overlap; final size is 32×32 pixels at 75% overlap. If the first correlation peak yields a spurious velocity vector, then it is replaced by the second, third or fourth highest correlation peak, whichever first satisfies the universal outlier median test [10]. The estimated bias error in SPIV measurement due to the experimental technique is up to $\simeq 3\%$ of the freestream velocity.

The ensemble-averaged statistics are based on a full batch of 3000 SPIV image pairs (at a sample rate of 2 Hz). The smallest resolvable length scale of velocity grid is $l_{yz} \simeq 0.45$ mm; this equates to $(L/7.3)/l_{yz} \simeq 608$ velocity vectors across the width of the hull. On the upper hull just above the casing where reflections are minimal, useful SPIV data are obtained as close as 10 mm (or $0.005L$) from the casing. For the mid/lower hull where stray reflections are significant, local masking of spurious vectors is up to 20 mm (or $0.010L$) away from the hull.

Ensemble-Averaged Velocity Field

In figures 1 and 2, the most prominent flow feature at 10° yaw is located downstream of the submarine cruciform on the upper hull. It is a system of three co-rotating vortices which is produced by the fin and the two hydroplanes. The leeward flow is on the starboard side. As viewed from downstream of the hull, the mean rotation direction of the vortex system is clockwise.

Figure 2(a, b) shows an enlarged view of the flow on the upper hull at $Re_L = 4 \times 10^6$; a similar flow is observed at $Re_L = 8 \times 10^6$. Here, the ensemble mean and root-mean-square (r.m.s.) resultant velocities are expressed non-dimensionally as $\langle \overline{U}_{xyz} \rangle / U_\infty$ and $\langle u_{xyz} \rangle / U_\infty$ respectively, where an angle bracket $\langle \ldots \rangle$ denotes the full-batch ensemble average. The wake of the fin is visible in figure 2 as a region of low velocity ($\langle \overline{U}_{xyz} \rangle / U_\infty < 1.00$) and high turbulence intensity ($\langle u_{xyz} \rangle / U_\infty > 0.06$) relative to the freestream. The wake rolls up to form a fin-tip vortex, where the mean velocity reaches up to $\langle \overline{U}_{xyz} \rangle / U_\infty \simeq 1.17$. At the centre of the fin-tip vortex, the turbulence intensity does not exceed $\langle u_{xyz} \rangle / U_\infty \simeq 0.40$. Figure 3 provides examples of horizontal y distribution of flow through the centre of the fin-tip vortex. The vortex core is defined as a region of flow where the turbulence intensity is no less than 20%-30% of the maximum intensity at the core centre, where the core diameter is $\simeq 1\% L$; see figure 3.

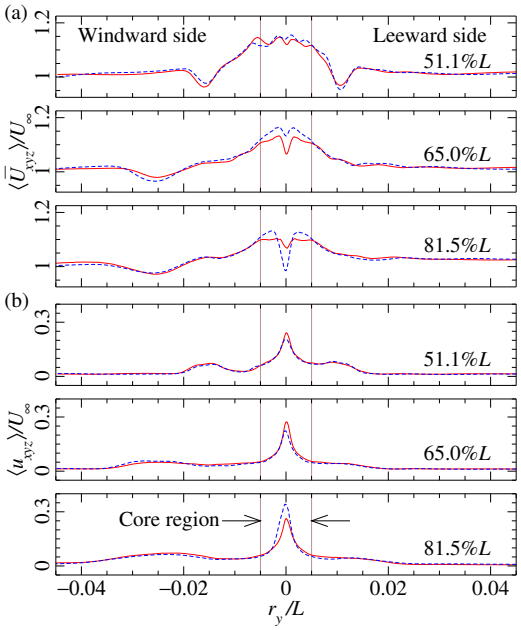

Figure 3. Horizontal y profile of the fin-tip vortex with (a) mean and (b) r.m.s. resultant velocities as functions of radial distance r_y/L from the fin-tip vortex centre; $Re_L = 4 \times 10^6$ (—) and 8×10^6 (- - -).

Cross-Stream Reynolds Stress

In figure 2(c), the shear layer of the fin wake is well defined by the cross-stream Reynolds stress $\langle u_x u_y \rangle / U_\infty^2$. The Reynolds stress is positive on the windward side of the shear layer and is negative on the leeward side. By tracing the boundary $\langle u_x u_y \rangle = 0$ between the positive and the negative Reynolds stresses, the locations of the fin-wake centreline are identified in figure 4.

Streamwise Component of Vorticity

In figure 4, the vortices are visualised by plotting the ensemble-averaged streamwise component of vorticity:

$$\langle \omega_x \rangle = \frac{\partial \langle \overline{U}_z \rangle}{\partial y} - \frac{\partial \langle \overline{U}_y \rangle}{\partial z}. \qquad (1)$$

The vorticity is calculated by using a finite central difference scheme in Tecplot 360 EX software and the results are non-dimensionalised as $\langle \omega_x \rangle r_m / U_\infty$, where $r_m = L/(2 \times 7.3)$ is the maximum radius of the hull. In figure 4, the negative vorticity

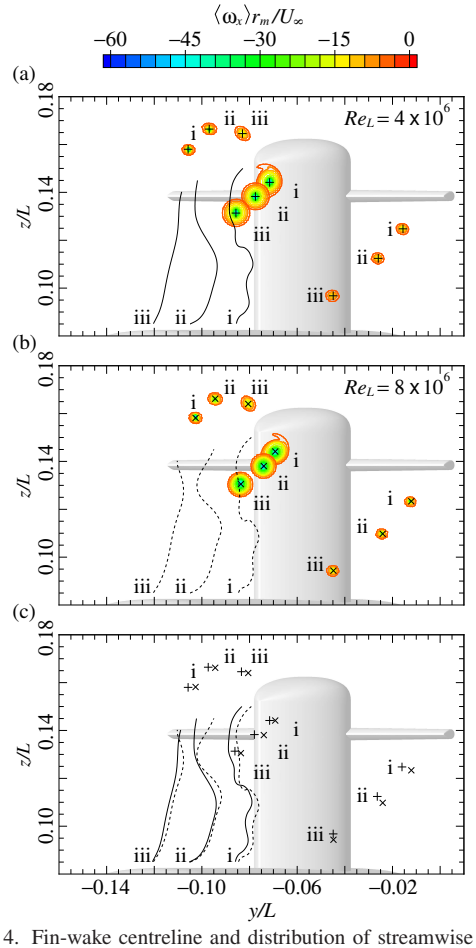

Figure 4. Fin-wake centreline and distribution of streamwise component of vorticity $\langle \omega_x \rangle r_m / U_\infty$ for cross-sectional planes at (i) $51.1\% L$, (ii) $65.0\% L$ and (iii) $81.5\% L$. Negative vorticity denotes clockwise rotation; (a)-(c) $Re_L = 4 \times 10^6$ (—, +) and 8×10^6 (- - -, ×).

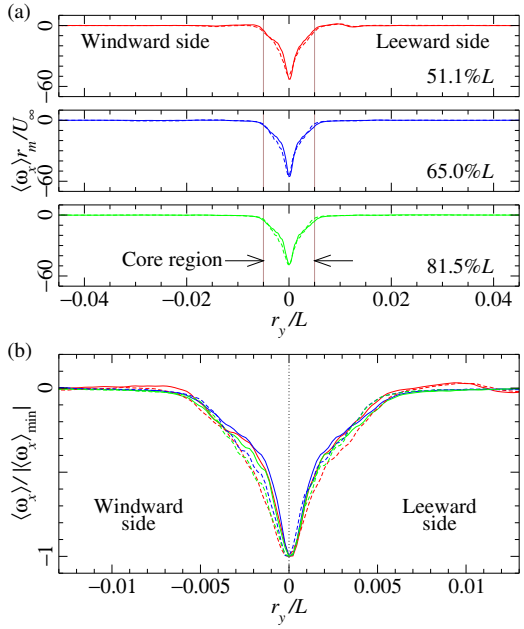

Figure 5. Horizontal y profile of the fin-tip vortex with (a) the streamwise component of vorticity as a function of radial distance r_y/L from the fin-tip vortex centre. (b) Self-similarity of vortex core measured at $Re_L = 4\times10^6$ (— 51.1%L, — 65.0%L, — 81.5%L) and 8×10^6 (- - - 51.1%L, - - - 65.0%L, - - - 81.5%L).

defines clockwise rotation; the local minima define the vortex centres, where their coordinates are given in table 1.

Figure 5 shows that, for the three downstream planes tested at $Re_L = 4\times10^6$ and 8×10^6, the non-dimensionalised vorticity distribution for the fin-tip vortex is self-similar. To obtain a clear boundary of the vortex core (of area A), the background vorticity is removed by setting the threshold level at $\langle\omega_x\rangle r_m/U_\infty = -5$. By integrating over the area of concentrated vorticity, this gives the circulation of the vortex core:

$$\kappa = \frac{|\Gamma|}{r_m U_\infty \sin(\psi)}, \quad \text{where} \quad \Gamma = \iint_A \langle\omega_x\rangle\, dA. \qquad (2)$$

The values of κ averaged over the three downstream planes are summarised in table 1. The circulation is strongest from the fin ($\overline{\kappa}_{\rm f}$) followed by the windward hydroplane ($\overline{\kappa}_{\rm hp,w}$) and the leeward hydroplane ($\overline{\kappa}_{\rm hp,l}$). By increasing Re_L from 4×10^6 to 8×10^6, the circulation of the vortex system increases by $\simeq 3\%$ (i.e. from $\Sigma\overline{\kappa} = \overline{\kappa}_{\rm f} + \overline{\kappa}_{\rm hp,w} + \overline{\kappa}_{\rm hp,l} = 1.797$ to 1.846) and the fin wake moves leeward by up to $0.5\%L$; see figure 4.

Conclusions

Low-speed wind-tunnel testing on a new 2 m long DST model (BB2) at a yaw angle (ψ) of 10° has identified a system of wake vortices on the upper hull of the model. The vortices are produced by a cruciform appendage which consists of a vertical fin and two horizontal hydroplanes. From ensemble averages of 3000 instantaneous SPIV measurements, the fin wakes are similar at Re_L of 4×10^6 and 8×10^6. For cross-sectional SPIV planes located at 51.1%, 65.0% and 81.5% of the model length, the vortex circulation is strongest from the fin, followed by the windward hydroplane then the leeward hydroplane.

Acknowledgements

Thanks go to the DST Experimental Aerodynamics Team and QinetiQ for submarine model design and manufacturing, wind-tunnel operations and SPIV traverse automation. Financial support from DST Maritime Division is acknowledged.

Table 1. Summary of vortex system on the upper hull. The uncertainty in y/L and z/L measurements is $\pm 2l_{yz}/L$ (or $\simeq \pm 0.00045$). The coordinates correspond to the local minima in vorticity; see figure 4.

Coordinates & Circulation of the upper-hull vortices			Fin	Hydroplanes	
				Windward	Leeward
$Re_L =$ 4×10^6	51.1%L	y/L	−0.072	−0.106	−0.016
		z/L	0.144	0.158	0.125
	65.0%L	y/L	−0.078	−0.097	−0.026
		z/L	0.138	0.166	0.112
	81.5%L	y/L	−0.086	−0.083	−0.045
		z/L	0.131	0.165	0.097
	Circulation averaged over the 3 SPIV planes		$\overline{\kappa}_{\rm f} =$ 1.460 ±0.071	$\overline{\kappa}_{\rm hp,w} =$ 0.216 ±0.009	$\overline{\kappa}_{\rm hp,l} =$ 0.121 ±0.012
$Re_L =$ 8×10^6	51.1%L	y/L	−0.069	−0.103	−0.013
		z/L	0.144	0.158	0.123
	65.0%L	y/L	−0.074	−0.094	−0.024
		z/L	0.138	0.166	0.109
	81.5%L	y/L	−0.084	−0.080	−0.045
		z/L	0.130	0.164	0.094
	Circulation averaged over the 3 SPIV planes		$\overline{\kappa}_{\rm f} =$ 1.473 ±0.078	$\overline{\kappa}_{\rm hp,w} =$ 0.245 ±0.011	$\overline{\kappa}_{\rm hp,l} =$ 0.128 ±0.005

References

[1] Anderson, B. *et al.*, Experimental and computational investigation of a generic conventional submarine hull form, in *29th Symposium on Naval Hydrodynamics*, Gothenburg, Sweden, 2012.

[2] Fureby, C. *et al.*, Experimental and numerical study of a generic conventional submarine at 10° yaw, *Ocean Engineering*, **116**, 2016, 1–20.

[3] Henbest, S. M. and Jones, M. B., *Transition on a generic submarine model*, Defence Science and Technology, Australia, 2018, in preparation.

[4] Jones, M. B., Erm, L. P., Valiyff, A. and Henbest, S. M., *Skin-friction measurements on a model submarine*, Defence Science and Technology, Australia, 2013, TR2898.

[5] Joubert, P. N., *Some aspects of submarine design part 2: shape of a submarine 2026*, Defence Science and Technology, Australia, 2006, TR1920.

[6] Kumar, C., Manovski, P. and Giacobello, M., Particle image velocimetry measurements on a generic submarine hull form, in *Proceedings of the 18th Australasian Fluid Mechanics Conference*, Launceston, Australia, 2012, paper 188.

[7] Lee, S.-K., *Topology model of the flow around a submarine hull form*, Defence Science and Technology, Australia, 2015, TR3177.

[8] Lee, S.-K., Giacobello, M., Manovski, P. and Kumar, C., Optimising camera arrangement for stereoscopic particle image velocimetry, in *Proceedings of the 19th Australasian Fluid Mechanics Conference*, Melbourne, Australia, 2014, paper 39.

[9] Overpelt, B., Nienhuis, B. and Anderson, B., Free running manoeuvring model tests on a modern generic SSK class submarine (BB2), in *Pacific International Maritime Conference*, Sydney, Australia, 2015.

[10] Westerweel, J. and Scarano, F., Universal outlier detection for PIV data, *Exp. Fluids*, **39**, 2005, 1096–1100.